nature physics

FOCUS | PERSPECTIVE

https://doi.org/10.1038/s41567-020-0906-9

Superconductivity and strong correlations in moiré flat bands

Leon Balents[1,2] ✉, Cory R. Dean[3], Dmitri K. Efetov[4] ✉ and Andrea F. Young[5] ✉

Strongly correlated systems can give rise to spectacular phenomenology, from high-temperature superconductivity to the emergence of states of matter characterized by long-range quantum entanglement. Low-density flat-band systems play a vital role because the energy range of the band is so narrow that the Coulomb interactions dominate over kinetic energy, putting these materials in the strongly-correlated regime. Experimentally, when a band is narrow in both energy and momentum, its filling may be tuned in situ across the whole range, from empty to full. Recently, one particular flat-band system—that of van der Waals heterostructures, such as twisted bilayer graphene—has exhibited strongly correlated states and superconductivity, but it is still not clear to what extent the two are linked. Here, we review the status and prospects for flat-band engineering in van der Waals heterostructures and explore how both phenomena emerge from the moiré flat bands.

Strongly correlated quantum many-body systems have provided the setting for many paradigm-shifting experimental discoveries; for example, the discovery of the fractional quantum Hall effect[1] led to a conceptual revolution, introducing the notion of topological order to characterize states of matter[2]. At the same time, in strongly correlated high-density materials, the large intrinsic energy scale of Coulomb interactions (the Coulomb energy $E_C \propto e^2/a$, where e is the electron charge, and a is a typical inter-electron distance, of atomic size) is of the order of thousands of kelvin, making strongly correlated phenomena candidates for room-temperature applications. Famously, superconductivity arising from electronic correlations (rather than electron–phonon coupling), manifests at temperatures tantalizingly close to room temperature[3]. Progress in understanding and exploiting such strongly correlated materials is hampered by their complexity[4]: diverse experimental phenomena often manifest simultaneously, complicating efforts to relate experimental systems to tractable theoretical models. The key experimental roadblock is the lack of ability to tune parameters in situ to obtain a broad view, and the challenge to theory is to identify the essential degrees of freedom to capture the physics and render predictive quantitative theory tractable. As we describe in this Perspective, many of these requirements can be met in van der Waals heterostructures, which permit the realization of highly controllable model Hamiltonians that feature many of the essential elements of a strongly correlated system. Recently, heterostructures of two-dimensional materials have emerged as a platform in which to investigate these questions, because, as we shall discuss, they feature highly tunable flat bands where the correlations are strong, and superconductivity may appear.

Flat bands are advantageous because they guarantee a large density of states, which amplifies the effects of interactions. When the effective Coulomb interaction energy E_C exceeds the band width W, even weak interactions can play a dominant role, lifting the near degeneracy between states occupying different combinations of single particle levels near the Fermi energy. Experimentally, flat-band engineering can bring strong interaction physics to low density electron systems where electrostatic gating can be used to control the density over the entire band. As a tradeoff, low electron density comes at the price of stringent requirements on sample disorder to avoid trivial localization of electrons, which suppresses correlation physics.

Van der Waals heterostructures consist of layered stacks of two-dimensional atomic crystals such as graphene, hexagonal boron nitride, and transition metal chalcogenides. Using aligned transfer of individual layers, complex heterostructures can be created with monolayer control over layer thickness and subdegree control of interlayer alignment[5–7]. This in turn provides wide-ranging opportunities for designing the effective electronic bandstructures in these systems. Here, we focus on moiré systems, in which a small mismatch in periodicity—introduced either by lattice mismatch or rotational misalignment—results in a long wavelength superlattice. Under the right circumstances, the resulting superlattice minibands can become exceptionally flat, causing correlation physics to manifest experimentally by the emergence of new ground states at partial band filling.

In particular, data on magic angle twisted bilayer graphene (tBLG) raises several key questions that are germane to observations of correlated states in van der Waals heterostructures more generally. What is the nature of the insulating states? Elementary considerations suggest they break one or more symmetries—but which ones? What is the origin and nature of the observed superconductivity? How strong are analogies to other correlated electronic systems, such as partially filled Landau levels and doped Mott insulators like the high-temperature superconducting cuprates? In the remainder of this Perspective, we focus on the phase diagram of tBLG, the best studied moiré flat-band system to date, and paint a picture of the current ability of the field to address these issues.

Landau levels and Hofstadter bands

Historically, Landau levels provide the paradigmatic example of two-dimensional flat bands. Landau levels arise when a clean two-dimensional system is subjected to a strong magnetic field. There, electronic motion is reduced to quantized cyclotron orbits by the Lorentz force, with the translational degeneracy giving rise to perfectly flat bands. The bandwidth of a Landau level is determined entirely by the degree of disorder, placing a premium on homogeneity. First studied in semiconductor heterostructures,

[1]Kavli Institute of Theoretical Physics, University of California, Santa Barbara, CA, USA. [2]Canadian Institute for Advanced Research, Toronto, Ontario, Canada. [3]Department of Physics, Columbia University, New York, NY, USA. [4]ICFO – Institut de Ciencies Fotoniques, The Barcelona Institute of Science and Technology, Barcelona, Spain. [5]Department of Physics, University of California, Santa Barbara, CA, USA. ✉e-mail: balents@kitp.ucsb.edu; dmitri.efetov@icfo.eu; andrea@physics.ucsb.edu

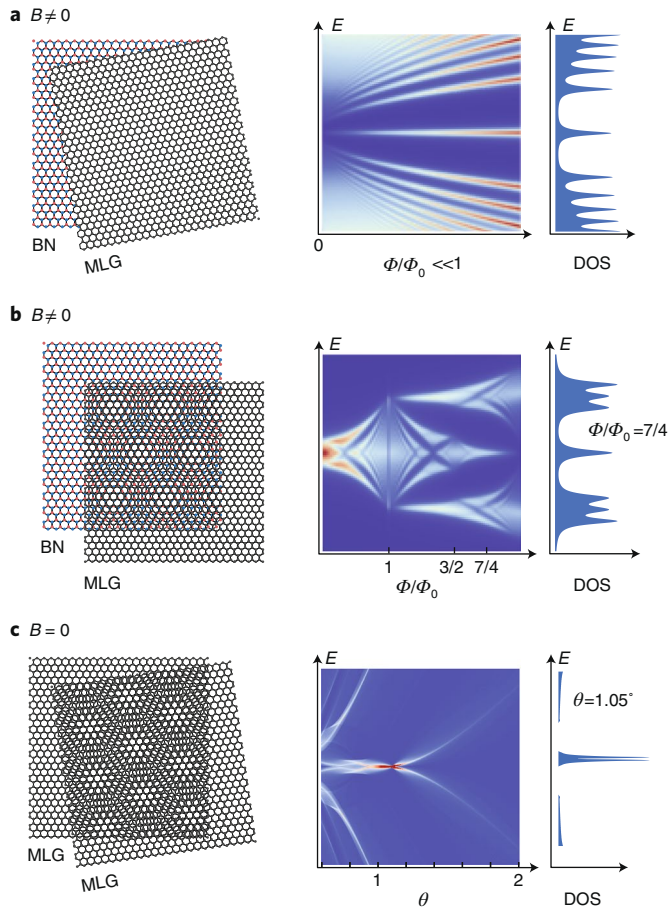

Fig. 1 | Three classes of flat bands in van der Waals heterostructures. a, In monolayer graphene (MLG) misaligned to hexagonal boron nitride (BN) (top panel), large magnetic fields (B) produce Landau levels (right panel, which depicts the single particle density of states (DOS) as a function of energy E). The prototypical flat band, partially filled Landau levels host intricate competition between topologically ordered fractional quantum Hall states, electron solids and isospin ferromagnets. Landau levels occur when the magnetic field is weak, and much less than one flux quantum threads each unit of the graphene lattice ($\Phi/\Phi_0 \ll 1$, where Φ is the flux per unit cell, and Φ_0 is the flux quantum). Besides their narrow bandwidth, Landau levels are known for their Chern number, which is equal to one, and high Berry curvature. **b**, Graphene rotationally aligned to hexagonal boron nitride. The interplay of a moiré superlattice potential, resulting from lattice mismatch between graphene and hexagonal boron nitride, together with a magnetic field, produces Hofstadter minibands. Tuning Φ/Φ_0 can create exceptionally narrow minibands, which may have arbitrary Chern number. **c**, Zero-magnetic-field flat bands in twisted bilayer graphene. Here the interplay of interlayer tunnelling and angle-induced momentum mismatch produces narrow bands in a range of twist angles (θ) near $\theta \approx 1.1°$. Flat bands include new features, such as valley-contrasting Chern numbers, which necessarily cancel by time-reversal symmetry.

partially filled Landau levels host a rich landscape of competing orders including ferromagnetism, charge-ordered stripe and bubble phases, and most famously the fractional quantum Hall liquids (Fig. 1a). A salient feature of these states is their intrinsic Berry curvature, which underlies their topological character and leads to integer and fractional quantum Hall effects. Theoretically, the Landau level problem is more tractable than other many-body systems. When the Landau level separation exceeds E_C, Coulomb interactions may be projected into the subspace of a single Landau level, vastly simplifying modeling. This has led to a remarkable quantitative agreement between experiment and numerical calculations for correlated phenomena occurring in a partially filled Landau level.

We begin this Perspective by tracing the development of correlated physics in moiré flat bands. The first experiments exploiting this phenomena combined moiré superlattice potentials with a magnetic field. In the absence of interactions, the interplay of the two generates the Hofstadter butterfly energy spectrum[8], defined by a recursive structure (fractal) of minibands[9–11]. Within this spectrum, fine-tuning of magnetic field and lattice potential can be used to create flat, isolated energy bands (Fig. 1b) dominated by electronic correlations[12–14]. More recently, moiré engineering has been used to successfully realize tunable flat-band physics in the absence of applied magnetic fields in a number of diverse materials systems[15–20]. For example, in twisted bilayer graphene, interlayer rotational misalignment of $\theta \approx 1.1°$ produces an isolated narrow band[21–23] (Fig. 1c).

Hofstadter bands present a theoretically tractable example of how the moiré lattice can enrich correlation physics. Figure 2a shows a detail of the Hofstadter spectrum in a graphene bilayer aligned to hexagonal boron nitride. The evolution of the Hofstadter bands with applied magnetic field is controlled by the number of magnetic flux quanta per moiré unit cell, n_ϕ. For rational $n_\phi = p/q$, each Landau level splits into p subbands. As in the Landau levels, the subbands have finite Chern number; this is reflected in the quantized Hall conductivity, te^2/h, that characterizes each gap in the spectrum, where t is an integer. The Hofstadter minibands differ from the Landau levels in several ways. First, the Chern number C of the Hofstadter minibands can take on any integer value. Second, Hofstadter bands are characterized by a second integer quantum number, s, which encodes the charge per unit cell. Finally, the minibands have finite intrinsic bandwidth and nontrivial momentum space structure, as evident in the energy-momentum dispersion of the $C = -1$ minibands shown in Fig. 2b.

As demonstrated in Landau level physics, the strength of interactions must be compared to the width of the low energy bands—correlations become strong when the product of E_C and the density of states (which is of the order of $1/W$; Fig. 1) is large. When the bandwidth of Hofstadter bands becomes small enough, the infinite recursion of the single-particle spectrum is cutoff. Instead, correlated insulating states appear at partial fractional fillings of the Chern bands. To date, several of these states have been observed; they are typically bulk insulators but have a quantized Hall conductivity. Some show integer t and fractional s; these are associated with a charge density wave like state that breaks the moiré lattice symmetry[12], multiplying the area of the effective unit cell. Others are more exotic, showing a fractionally quantized Hall conductivity as well as a fractional s. With sufficient experimental input, numerical methods developed for Landau levels have been adapted to incorporate this lattice, confirming a robust phase space for fractional Chern insulators. Remarkably, fractional Chern insulators localize a fractionally charged anyon to each moiré superlattice cell[13], potentially enabling new techniques to control exotic quasiparticles through lattice defects[24,25].

The appearance of insulators at integer fillings where band theory would predict metals is a powerful identifier for correlated insulators; it applies in traditional quantum materials like transition metal oxides, where these are usually called Mott insulators[26], as well as to quantum Hall ferromagnets at integer filling within Landau levels endowed with internal degeneracy. We refer to such states as correlated insulators. The first sign of interactions in tBLG near the magic angle (as well as in other moiré flat-band systems, discussed at the end of this Perspective) was similarly the observation of insulating states or metallic resistivity peaks at partial band filling corresponding to an integer number of electrons per unit cell[16]. While zero-field moiré flat bands resemble Landau Levels and Hofstadter minibands in some ways, the absence of an orbital

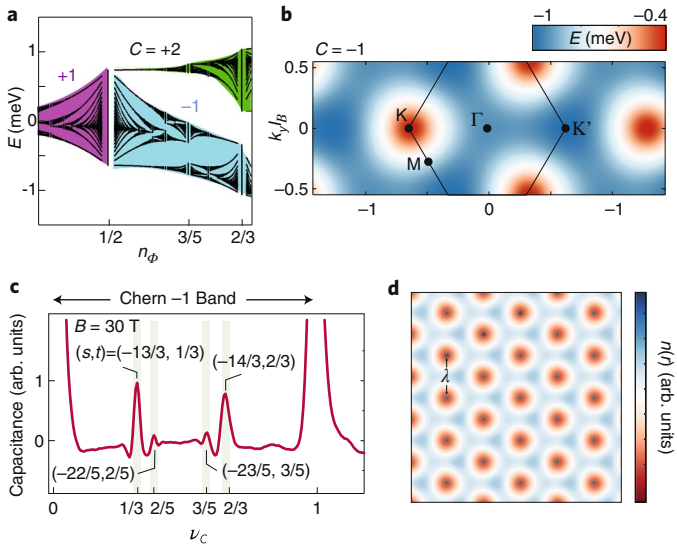

Fig. 2 | Correlation-driven phases in Hofstadter flat bands. a, Section of the Hofstadter energy (E) spectrum for bilayer graphene on hexagonal boron nitride, plotted as a function of number of magnetic flux quanta per moiré unit cell n_ϕ for a moire potential strength of 10 meV. **b**, Energy-momentum dispersion of the $C = -1$ energy band at $n_\phi = 2/3$ (the axes are cartesian coordinates of momentum, k_x, k_y, times the magnetic length l_B). **c**, Capacitance measured across the lower $C = -1$ band (ν_C is the filling factor of the band) . Instead of a continuation of the hierarchy of mini-gaps predicted by the single particle model, experiments show correlated insulating states at fractional filling of the Chern band. In the $C = -1$ band depicted, they are fractional Chern insulators, characterized by fractionally quantized Hall conductivity and fractional charge bound to each moiré unit cell[13]. **d**, Real-space map of charge density $n(r)$ for a fractional Chern insulator ground state, calculated by density matrix renormalization group[82] at $n_\phi = 2/3$ for the bands shown in **a**, **b**. Figure adapted with permission from: **a**, **c**, **d**, ref. [13], AAAS.

magnetic field significantly expands the accessible phase diagram. An exciting demonstration of the novelty of $B = 0$ flat bands is the observation of superconductivity—for which magnetic fields are anathema—at partial band filling[27–29]. Also unique to the zero-field flat-band systems is the appearance of insulating states that spontaneously break time-reversal symmetry[30,31]—impossible to observe in flat bands, such as Hofstadter mini-bands, that only appear under large magnetic fields

Twisted bilayer graphene

A theoretical perspective on tBLG requires an understanding of both bands and interactions. The band structure involves two small parameters: the wavevector k_m of the moiré pattern and the strength of the coupling w between incommensurate layers. Generically, $k_\mathrm{m} a_0 \ll 1$ and $w/t \ll 1$, where a_0 is the inter-atomic distance, and t is the strength of intra-layer hopping or atomic bandwidth. This enables a continuum band description[21,23], in which the dimensionless parameter $\alpha = vk_\mathrm{m}/w$ measures the degree of band reconstruction by the moiré pattern (v is the graphene Dirac velocity). Exceptionally flat bands occur in tBLG for narrow ranges of $\alpha \gtrsim 1$, which correspond to the magic angles, a theoretical prediction that motivated early experimental efforts[15,16,27] (Fig. 3a,c). In addition to their flatness, the moiré bands possess incipient Berry curvature, arising from the original Dirac points of the graphene constituents[32]. This feature, not found in any known high-density correlated material to the authors' knowledge, allows topology to naturally enter tBLG physics[33–35].

Addressing the many-body ground states of tBLG in full generality is theoretically challenging. However, the extreme low density of electrons implies one simplification: Coulomb interactions conserve to an excellent approximation spin and charge of each valley separately, and also allow valley interchange via time-reversal symmetry. This emergent $U(2) \times U(2) \times Z_2$ spin–valley symmetry has implications for symmetry breaking states and their excitations, similar to those studied in graphene quantum Hall ferromagnets. Following the Landau level analogy, a Hartree–Fock approximation, which fills renormalized bands chosen to minimize the total energy, can explain insulating states at integer filling factors without enlarging the moiré unit cell.

Within Hartree–Fock theory, these correlated insulators must break some symmetry, in order that the band filling is consistent with a gap at the Fermi energy. At charge neutrality the only requirement is that the Dirac degeneracy of conduction and valence bands is removed. This may be minimally accomplished by breaking the C_2T symmetry (time-reversal T combined with a two-fold rotation C_2 around the axis normal to the bilayer) of ideal tBLG which locally protects Dirac points, but Dirac points may also be removed by pair annihilation via large C_3-breaking deformations (C_3 denotes three-fold rotation symmetry normal to the layers). In a practical experimental situation, the C_2T symmetry is always broken explicitly to some degree by the layers of hexagonal boron nitride that encapsulate the tBLG. The more general case can be described in terms of the parameter ν, the filling, that labels how many of the moiré minibands are filled. At $\nu = \pm 2$, in addition, the four-fold band degeneracy must be halved in a correlated insulator, most simply by breaking either spin or valley degeneracy. At $\nu = \pm 1, \pm 3$, the filling constraints are most severe, and both spin and valley degeneracy must be lifted in a correlated insulator.

These filling constraints still allow a large number of possible symmetry breaking patterns, breaking spin and valley symmetries in different ways (for example, valley polarization versus inter-valley coherence) and interweaving them with space group operations (for example orbital–spin ferromagnetism versus antiferromagnetism or density waves and multipolar orders). The competition between different potential orders is keen and difficult to resolve unambiguously, and indeed theoretical studies reveal diverse results that depend on the assumptions in the model[36–42]. Experimental results too have a high sensitivity to detail. Figure 3 shows a comparison between two tBLG devices near the magic angle, which differ primarily in the alignment of the tBLG to one of the hexagonal boron nitride encapsulant layers. The unaligned device[29] shows insulating states at $\nu = -2, 0, 2$ and 3 in addition to a weak resistivity peak at $\nu = 1$; in contrast, the device with aligned hexagonal boron nitride shows insulating behavior only at $\nu = 0$, a weak resistivity peak at $\nu = 2$ and a quantized anomalous Hall effect at $\nu = 3$.

While disorder likely plays some role in sample variability, focusing on data at $\nu = 3$ in the devices of Fig. 3 leaves little doubt that small modifications to the single-particle structure are sufficient to tilt the balance between competing states, with both devices showing behavior indicative of *clean* insulating or quantum Hall physics at the same filling. These observations are natural within the theoretical framework of moiré bands, for which variations like strain, alignment with a hexagonal boron nitride substrate, and twist angle can create or modify Chern bands and thereby change the ground state[36]. At this stage, a Hartree–Fock picture of the correlated insulators appears mostly consistent with experimental data, though we note that other approaches are possible and a more nuanced perspective may yet emerge. Regardless, the sensitivity to device details suggests that the first task for ab initio theory of the correlated insulators should not be to predict specific insulating states, but rather to predict the set of insulators with competitive energy at a given filling factor, and to explain which perturbations favor which states within this set.

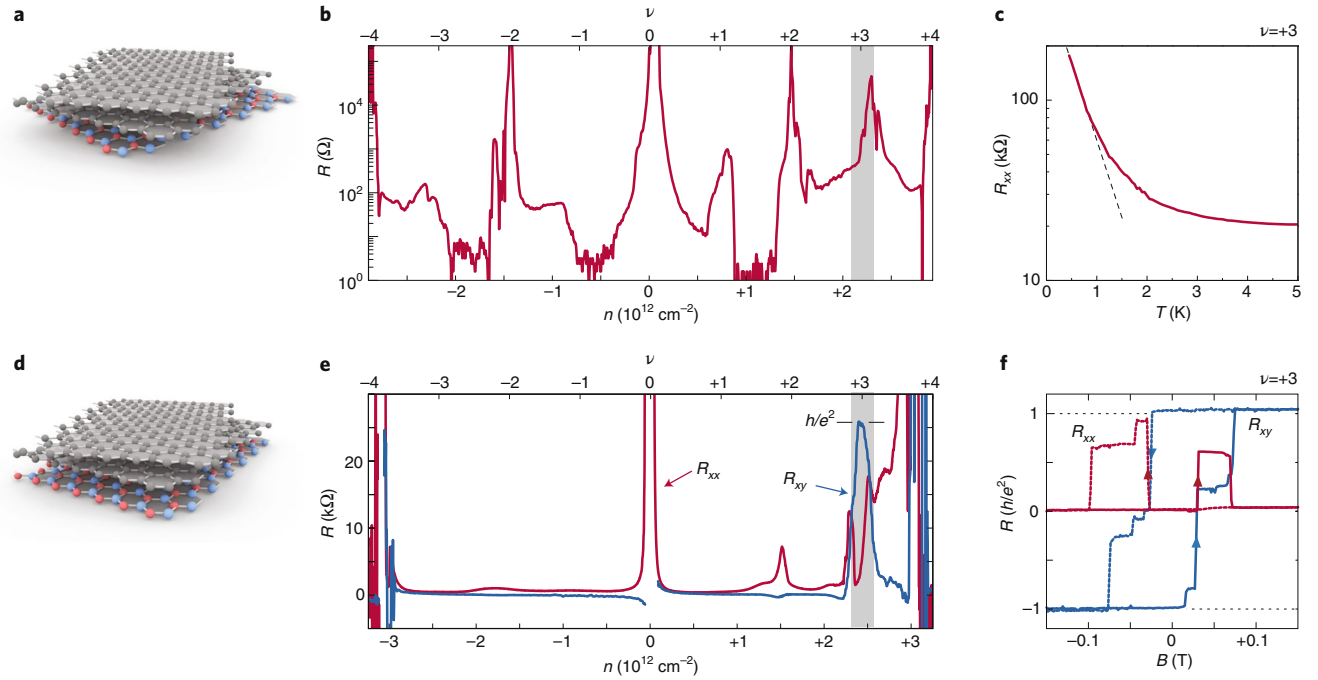

Fig. 3 | Substrate tuning of electronic structure in twisted bilayer graphene. a, Schematic of a tBLG rotationally misaligned to a hexagonal boron nitride substrate. **b**, Experimental data for a misaligned device. High-resistivity correlated insulating states are observed at fillings $\nu = -2, 0, +2$, and $+3$, in addition to superconducting states over intermediate ranges of $\nu \in (-3, -2)$, $(-1, 0)$, and $(+1, +2)$. Absolute electron density n is shown on the bottom horizontal axis. **c**, Thermally activated behavior is observed $\nu = +3$ in misaligned devices[28,29]. **d**, Schematic of a tBLG rotationally aligned to a hexagonal boron nitride substrate. **e**, Experimental data for an aligned device. Besides an insulator at $\nu = 0$, only a weakly resistive peak is observed at $\nu = +2$. In addition, and quantum anomalous Hall state appears at $\nu = +3$, showing vanishing diagonal resistance R_{xx} and quantized Hall resistance R_{xy}. **f**, Response at $\nu = +3$ in an aligned device, showing magnetic hysteresis and a quantized Hall response stable at $B = 0$. Figure adapted with permission from: **b**, **c**, ref. [29], Springer Nature Ltd; **e**, **f**, ref. [31], AAAS.

Superconductivity

We next turn to superconductivity in tBLG. A superconductor (SC) is intrinsically beyond a Hartree–Fock description and is a clear departure from quantum Hall ferromagnetism. Moreover, whereas the correlated insulators are most easily understood as consequences of the Coulomb repulsion alone, superconductivity may arise from either an all-electronic mechanism[43–47] or a more conventional, BCS-like phonon-mediated interaction[48–50]. Identifying the underlying mechanism of superconductivity is, at present, the major outstanding question in this field. To date, however, progress on this issue has been slowed by the challenge of understanding the experimental phase diagram.

The first difficulty is that two-dimensional superconductors are not expected to show a detectable Meissner effect, making identification of superconductivity more challenging than in their three-dimensional counterparts. Moreover, high mobility devices can exhibit ballistic and phase coherent transport at low temperature[6,51], providing a mechanism for observing zero resistance unrelated to superconductivity. In moiré systems superconductivity has generally been defined by the simultaneous observation of two characteristic transport signatures: a zero-resistance state that is rapidly suppressed with temperature and magnetic field, and measurement of a field-dependent critical current. We show some examples in Fig. 4. In some devices, further evidence of superconductivity is provided by oscillations in the critical current versus magnetic field, interpreted as mesoscopic quantum interference arising from the presence of insulating or normal metal weak links related to spatial variations in the moiré pattern or charge disorder. In this picture, superconductivity is percolative[27–29]. In this still rapidly developing field, some devices—at this point restricted to tBLG[27–29,52,53]—show all of these signatures. In others, a sharp decrease in the resistivity upon lowering temperature, often saturating to non-zero value, together with a non-linear I–V response, has been interpreted as evidence of superconductivity[19,54–57]. In these cases, the non-zero resistance is generally attributed to sample inhomogeneities and poor electrical contacts; however, it has also been suggested that such signatures can also be associated with isospin symmetry breaking transitions instead of true superconductivity[58].

A second major experimental challenge is to eliminate variability between devices. To date, only a handful of groups have reported evidence of superconductivity in tBLG (according to the metrics outlined above), and within these measurements, no two devices exhibit the same precise superconducting response. Instead, there are large variations observed in the critical temperature, critical magnetic field, critical current, and the density range over which the superconducting domes exist. As discussed above, some aspects of the lack of reproducibility clearly arise from extreme sensitivity to uniform strains, alignments to substrates, and minute variations in the twist angle itself. However, other aspects clearly represent inhomogeneities of samples. Inhomogenous strain effects between the individual graphene layers can induce strong spatial variations in the periodicity of the moiré lattice. This has been observed in microscopy studies where the moiré unit-cell area is routinely seen to vary on length scales comparable to the moiré wavelength[59–66]. Such twist-angle inhomogeneity has dramatic effects on transport measurements, which typically probe length scales of hundreds of moiré lattice constants. In the extreme case, strongly varying twist angle across the device area can lead to spatial separation of different phases. At densities compatible with superconductivity, phase separation leads to networks of superconducting and normal regions.

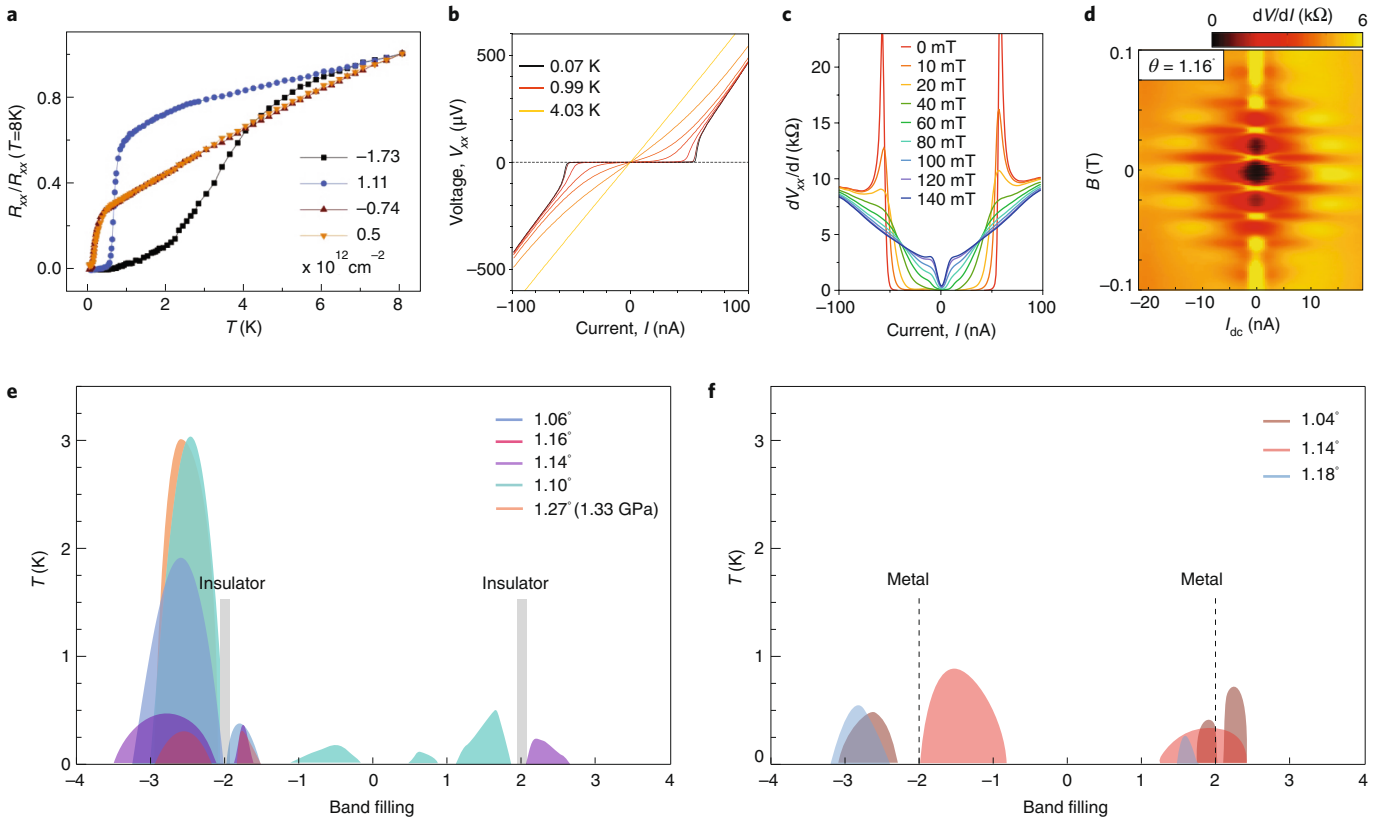

Fig. 4 | Superconductivity in twisted bilayer graphene. Evidence of superconductivity includes observation of zero resistance below a critical temperature (**a**), together with non-linear *V*–*I* curves (R_{xx} and V_{xx} and longitudinal resistance and voltage, respectively) showing a field- and temperature-tunable critical current (**b**, **c**). **d**, Oscillations of the critical current (I_{dc} is a d.c. current) versus magnetic field resemble Fraunhofer oscillations, providing further support for superconductivity while also suggesting the presence of sample inhomogeneities (see text). **e**, **f**, Cumulative phase diagram of superconducting domes appearing in the experimental literature. **e** includes devices in which superconductivity coexists simultaneously with insulating behaviour at band filling $\nu = \pm 2$. Superconducting pockets have been observed throughout the band but are are generally strongest near half filling. Twist angles include 1.06° (ref. [27]), 1.10° (ref. [29]), 1.14° (ref. [28]), 1.16° (ref. [27]) and 1.2° (ref. [28]). The device at 1.27° was measured under 1.33 GPa applied pressure to induce the flat band[28,83,84]. **f**, Devices in which superconducting domes appear in the absence of insulating behaviour at half band filling. Twist angles include 1.04° (ref. [52]), 1.1° (ref. [52]) and 1.18 (ref. [67]). Figure adapted with permission from: **a**, ref. [29], Springer Nature Ltd; **b**–**d**, ref. [27], Springer Nature Ltd.

Despite the role of inhomogeneities, we can achieve an understanding of the overall phase diagram of superconductivity by combining data from several studies published to date. Figures 4e–f show a phase diagram that includes data taken from seven superconducting devices, reported by four different research groups[27–29,52,67]. The devices have twist angles ranging from 1.04° to 1.18° (in addition to a device with $\theta \approx 1.27°$ that showed superconductivity under applied pressure[28]). The coloured domes indicate superconducting regions. Each device shows a unique landscape of superconductivity but some trends emerge in the overall angle dependence. For example, the superconducting transition temperature T_c (defined as the temperature corresponding to a 50% drop relative to the normal state resistance) is highest in devices with twist angles closest to 1.1°. Away from 1.1°, superconductivity is gradually suppressed, and superconductivity is not typically observed in devices with $\theta < 1.0°$ or $\theta > 1.2°$.

In the initial reports of superconductivity in tBLG[27,28], superconductors were observed in the center of the band, in the vicinity of correlated insulating states at $\nu = \pm 2$. In such devices, insulators win over superconductivity at integer filling positions, with superconductivity prevailing upon slight doping of the insulating phase. However, subsequent studies found superconductivity broadly distributed across the entire moiré band[29]. More recent experiments[52,67] showed that superconductivity may appear in the absence of correlated insulators (Fig. 3b) and even in the absence even of the $\nu = \pm 4$ insulating states[53] that mark the formation of an isolated low energy band. In these devices, strong superconductors are observed in the vicinity of $\nu = \pm 2$, with T_c values that are comparable to devices with well developed insulators.

These observations provide critical input to the question of the mechanism of superconductivity in tBLG. In the pioneering experiments, the apparent correlation between superconductors and correlated insulators[27] suggested a direct relation between these phases: in this picture, Cooper pairing could be mediated by excitations of the correlated insulators, in an all-electronic mechanism similar to that proposed for unconventional superconductors like the cuprates[68]. The more recent observations that superconductivity is decoupled from the appearance of the correlated insulators or even an isolated flat band casts doubt on this interpretation. In other theoretical scenarios, the correlated insulator and superconducting phases might not share a common microscopic mechanism, but rather compete. In this scenario, Coulomb interactions would drive the formation of the commensurate insulators while superconductivity might arise from a more conventional electron–phonon mechanism. An intermediate situation is also conceivable, that both insulators and superconductors are driven by Coulomb interactions but that the latter is not due to proximity of the former. Of course, the extreme sensitivity of electronic structure details also raises the possibility that the superconducting pairing mechanism may not be universal across all devices, or even across band fillings within

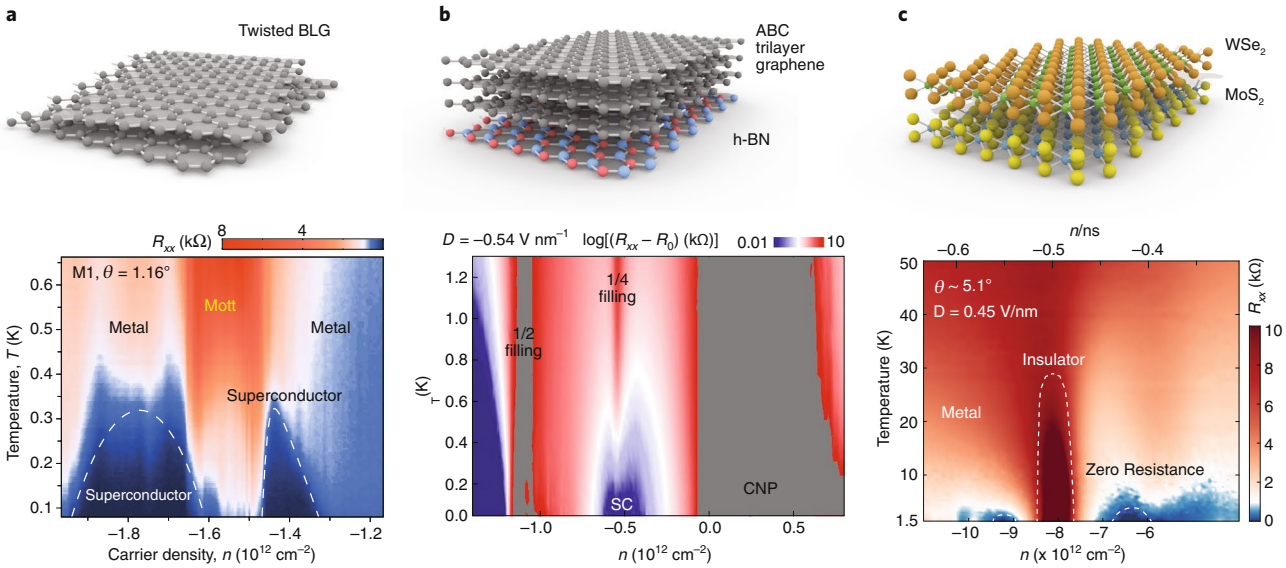

Fig. 5 | Proliferation of zero-field narrow-band systems. Narrow moiré bands arise in a variety of materials including **a**, twisted homo-bilayers of graphene[54,78–80], **b**, rhombohedral trilayer graphene aligned to hexagonal boron nitride[17,57,85] and **c**, homo- (as well as hetero-) bilayers of transition metal chalcogenides[18–20,81]. All show qualitatively similar features, including resistive states at commensurate fillings and robust or incipient zero-resistance states at other positions in the band. *D*, displacement field normal to the layers; ns, density of a full superlattice band; SC, superconductor; CNP, charge neutrality point. Figure adapted with permission from: **a**, ref. [27], Springer Nature Ltd; **b**, ref. [57], Springer Nature Ltd.; **c**, ref. [19].

a single device, although no experimental evidence supports this interpretation to date. The need for direct experimental probes of the superconductivity is pressing.

Future experiments on twisted bilayer graphene

Fabrication protocols are improving, as shown by transport studies that indicate twist-angle variations of only $\Delta\theta \sim 0.01°$ on 10-μm length scales[29]. Besides allowing higher resolution mapping of the superconducting phase diagram[28,29,52,67], these advances are essential first steps towards building more complex devices required for next generation experiments that directly probe the nature and origin of the superconducting states. For example, van der Waals heterostructures enable unique opportunities to investigate the many-body phase diagram as a direct function of interaction strength. Devices can be fabricated with metallic gates only a few nanometers from the tBLG layer. At this distance, image charges in the monolayer graphene are closer to the tBLG than the approximately 15-nm size of the Wannier orbitals[69–71], effectively screening the Coulomb interactions[52,72,73]. It is also possible to control, in situ, the screening length of carriers in tBLG. This can be achieved by replacing the metallic layer with a graphene monolayer, whose density of states (and thus its ability to screen the tBLG) can be modified by gating. This means that the screening length can be controlled from well above the moiré wavelength in the high-density regime of the monolayer to well below it at charge neutrality. The phase diagram of tBLG could then be studied as a function of interaction strength. Naively, enhancement of T_c with lowered Coulomb interaction would support pairing via electron–phonon interaction, which is not effectively screened. The first experiment in this direction[74], however, finds a small suppression of the superconducting dome near $\nu = -2$. This suggests that electron interactions are not necessarily inimical to superconductivity, either by reconstructing the underlying band structure or because the superconductivity arises from an electronic mechanism.

Experimental probes that may provide more definitive evidence for the existence of superconductivity are of the highest importance. These may include finite frequency measurements of the kinetic inductance, measurements of gate-controlled Josephson junctions, and probes of the Little–Parks effect in mesoscopic rings. The order parameter symmetry also remains unexplored in experiments. Is it singlet or triplet, and what is the spatial structure of the pair wave function? The enhanced spin–valley symmetry affords, a priori, an even richer characterization of superconducting pairing, involving spin, orbital and valley structure of the states. The observed suppression of superconductivity by an in-plane applied field[27] probably supports singlet pairing. Recently, indications of a more unconventional order parameter were reported in twisted double bilayer (which is two Bernal graphene bilayers stacked with twist angle between them, although there was no demonstration of phase coherence)[54]. Direct measurements of pairing symmetry have been successful in cuprate superconductors, typically effected using phase-sensitive measurements that permit comparison of the phase in the material of interest to that of a conventional *s*-wave superconductor[75].

Such experiments are readily applicable to tBLG, where high-transparency superconducting contacts are straightforward to integrate into the fabrication process. Thermal and spectroscopic probes are also sensitive to a superconducting gap; besides eliminating ambiguities as to the presence of superconductivity, these measurements can also identify the superconducting order parameter. In particular, some superconducting states proposed theoretically are topological, and may support chiral edge states or Majorana zero modes bound to vortices. Present experiments do not yet probe such subtle features, but the advent of scanning probe studies such as scanning tunneling microscopy[59–61] and nanoscale magnetic imaging[62] in tBLG may soon confirm or rule out these possibilities. Finally, homogeneous devices hosting both quantized anomalous Hall effects and superconductivity also enable gate-controlled interfaces between these states, which may host emergent Majorana boundary modes.

The correlated insulators and superconductors naturally hold center stage in both theory and experiment, as they represent sharply defined symmetry-breaking phases whose universal properties can be clearly addressed. However, tBLG also presents a remarkable

opportunity for quantitative study even in the 'normal' state where no symmetries are spontaneously broken. Notably, the longitudinal and Hall resistivity can be measured as a function of electron density and temperature over a range which would be unprecedented in high-density electronic materials: the bands closest to the Fermi energy can be completely emptied or filled, with a variation of more than eight electrons per moiré unit cell, and the temperature can be varied from far below the Fermi energy to above the full bandwidth of the conduction and valence bands, even becoming so large that higher bands may contribute to transport. This presents a model system for the study of transport in the presence of strong electron correlations. Experiments probing the high-temperature regime of tBLG, for instance, have found an enhanced linear-in-T resistivity in this system[76,77], indicating exceptionally strong scattering. Such behavior has often been interpreted in bulk materials as an indication of exotic physics, for example non-Fermi liquid states, quantum criticality and Planckian dissipation. Testing such scenarios requires detailed quantitative theory, and is complicated by the possibility of more prosaic explanations such as electron—phonon scattering, in some circumstances. The observation in tBLG presents an unprecedented opportunity for deep and quantitative understanding of the true physics underlying this behavior, taking advantage of the complete theoretical knowledge of graphene's electronic structure and interactions, and the vast in situ tunability of tBLG. We anticipate that, ultimately, a comprehensive understanding of normal state transport in tBLG structures should be obtainable, at a fully quantitative level beyond scaling arguments.

Other materials

The community is also making rapid progress in expanding the spectrum of flat band vdW heterostructures showing correlated behavior (Fig. 5b,c). This growing list includes twisted double-bilayer graphene (fabricated by co-laminating two Bernal bilayer graphene flakes with a rotational mismatch)[54,78–80], ABC-trilayer graphene (fabricated with zero angle alignment to a hexagonal boron nitride substrate—ABC denotes the stacking sequence)[17,57], and hetero- and homo-bilayer structures fabricated from semiconductor transition metal dichalcogenides[18–20,81]. All of these heterostructures share the common feature of a moiré superlattice on the length scale of 10 nm due to lattice or angle mismatch. Like tBLG, they show resistivity features at commensurate fillings of the lowest-lying moiré bands, and low-resistivity states that have been taken as evidence for superconductivity, despite diversity in the underlying constituent materials.

Of the moiré flat-band systems studied to date, all, with the exception of tBLG, are built from materials in which the low-energy bands of the constituent layers are comparatively flat even in the absence of the moiré superlattice. This leads to the experimental advantage that moiré minibands induced by the superlattice potential become flat for any small k_m so that the flat band condition is not restricted to a narrow range of 'magic' parameters but instead obtains for a range of angles and displacement fields. This is indeed born out in the experiments that observe correlated features at integer ν over broad ranges of the parameter space. Remarkably, the presence of even a weak superlattice potential appears to be a necessary for the manifestation of dramatic correlation physics. This finding may point to the importance of band isolation for the formation of the correlated insulating states[79].

Conclusions

In summary, moiré van der Waals heterostructures have already demonstrated an exceptionally wide range of physical phenomena. What additional secrets might still be hidden in these materials? Superconductivity, correlated insulators, and even quantized anomalous Hall effects and topological order all have years- or decades-long histories of study and yet still hold fundamental mysteries. The moiré flat-band systems provide an exciting new platform to address these outstanding issues. In particular, the in-situ tunability available in these systems is unprecedented, enabling complete access to the associated phase diagram merely by applying electrostatic fields, rather than having to grow a new device for each new data point. The ability to realize flat bands under wide ranging scenarios provides an opportunity for identifying universal phenomena and distinguishing them from sample-specific effects. These newly available degrees of freedom also enable rich opportunities for new discovery.

One possible direction for future discovery is to leverage the exquisite control afforded by these systems over the microscopic Hamiltonians from which correlated phases emerge. This control could enable the observation of long-sought phases of matter, such as spin liquid or zero-field fractional Chern insulator ground states that are known to arise in toy models with a passing resemblance to some moiré heterostructures. On the experimental side, such control can be combined with measurements that are compatible only with two-dimensional devices, particularly those combining diverse local observables with the plethora of device geometries enabled by the two-dimensional platform. Perhaps most exciting is the possibility of new phase discovery beyond our current paradigm. It is worth remembering that the first experimental observation of the fractional quantum Hall effect was misidentified as a Wigner crystal[1], at the time a sought after phase of matter but one that had been theoretically understood for decades. Final understanding of the observations of Tsui and Stormer would give birth to our modern understanding of correlated quantum matter. Only time and effort, both theoretical and experimental, will tell if tBLG holds similar surprises.

Received: 3 December 2019; Accepted: 8 April 2020;
Published online: 19 May 2020

References

1. Tsui, D. C., Stormer, H. L. & Gossard, A. C. Two-Dimensional Magnetotransport in the Extreme Quantum Limit. *Phys. Rev. Lett.* **48**, 1559–1562 (1982).
2. Wen, X.-G. Topological orders and edge excitations in fractional quantum Hall states. *Adv. Phys* **44**, 405–473 (1995).
3. Bednorz, J. G. & Müller, K. A. Possible highTc superconductivity in the Ba-La-Cu-O system. *Z. Phys. B* **64**, 189–193 (1986).
4. Fradkin, E. & Kivelson, S. A. Ineluctable complexity. *Nat. Phys* **8**, 864–866 (2012).
5. Dean, C. R. et al. Boron nitride substrates for high-quality graphene electronics. *Nat. Nanotechnol* **5**, 722–726 (2010).
6. Wang, L. et al. One-Dimensional Electrical Contact to a Two-Dimensional Material. *Science* **342**, 614–617 (2013).
7. Kim, K. et al. van der Waals Heterostructures with High Accuracy Rotational Alignment. *Nano Lett.* **16**, 1989–1995 (2016).
8. Hofstadter, D. R. Energy levels and wave functions of Bloch electrons in rational and irrational magnetic fields. *Phys. Rev. B* **14**, 2239–2249 (1976).
9. Ponomarenko, L. A. et al. Cloning of Dirac fermions in graphene superlattices. *Nature* **497**, 594–597 (2013).
10. Dean, C. R. et al. Hofstadter's butterfly and the fractal quantum Hall effect in moiré superlattices. *Nature* **497**, 598–602 (2013).
11. Hunt, B. et al. Massive Dirac Fermions and Hofstadter Butterfly in a van der Waals Heterostructure. *Science* **340**, 1427–1430 (2013).
12. Wang, L. et al. Evidence for a fractional fractal quantum Hall effect in graphene superlattices. *Science* **350**, 1231–1234 (2015).
13. Spanton, E. M. et al. Observation of fractional Chern insulators in a van der Waals heterostructure. *Science* **360**, 62–66 (2018).
14. Cheng, B. et al. Fractional and Symmetry-Broken Chern Insulators in Tunable Moiré Superlattices. *Nano Lett.* **19**, 4321–4326 (2019).
15. Kim, K. et al. Tunable moiré bands and strong correlations in small-twist-angle bilayer graphene. *Proc. Natl Acad. Sci. USA* **114**, 3364–3369 (2017).
16. Cao, Y. et al. Correlated insulator behaviour at half-filling in magic-angle graphene superlattices. *Nature* **556**, 80–84 (2018).
17. Chen, G. et al. Evidence of a gate-tunable Mott insulator in a trilayer graphene moiré superlattice. *Nat. Phys* **15**, 237–241 (2019).
18. Regan, E. C. et al. Mott and generalized Wigner crystal states in WSe 2/WS 2 moiré superlattices. *Nature* **579**, 359–363 (2020).

19. Wang, L. et al. Magic continuum in twisted bilayer WSe2. Preprint at https://arxiv.org/abs/1910.12147 (2019).
20. Tang, Y. et al. Simulation of Hubbard model physics in WSe2/WS2 moiré superlattices. *Nature* **579**, 353–358 (2020).
21. Lopes dos Santos, J. M. B., Peres, N. M. R. & Castro Neto, A. H. Graphene bilayer with a twist: electronic structure. *Phys. Rev. Lett.* **99**, 256802 (2007).
22. Suárez Morell, E., Correa, J. D., Vargas, P., Pacheco, M. & Barticevic, Z. Flat bands in slightly twisted bilayer graphene: Tight-binding calculations. *Phys. Rev. B* **82**, 121407 (2010).
23. Bistritzer, R. & MacDonald, A. H. Moiré butterflies in twisted bilayer graphene. *Phys. Rev. B* **84** (2011).
24. Barkeshli, M. & Qi, X.-L. Topological Nematic States and Non-Abelian Lattice Dislocations. *Phys. Rev. X* **2**, 031013 (2012).
25. Knapp, C., Spanton, E. M., Young, A. F., Nayak, C. & Zaletel, M. P. Fractional Chern insulator edges and layer-resolved lattice contacts. *Phys. Rev. B* **99**, 081114 (2019).
26. Imada, M., Fujimori, A. & Tokura, Y. Metal-insulator transitions. *Rev. Mod. Phys.* **70**, 1039–1263 (1998).
27. Cao, Y. et al. Unconventional superconductivity in magic-angle graphene superlattices. *Nature* **556**, 43–50 (2018).
28. Yankowitz, M. et al. Tuning superconductivity in twisted bilayer graphene. *Science* **363**, 1059–1064 (2019).
29. Lu, X. et al. Superconductors, orbital magnets and correlated states in magic-angle bilayer graphene. *Nature* **574**, 653–657 (2019).
30. Sharpe, A. L. et al. Emergent ferromagnetism near three-quarters filling in twisted bilayer graphene. *Science* **365**, 605–608 (2019).
31. Serlin, M. et al. Intrinsic quantized anomalous Hall effect in a moiré heterostructure. *Science* **367**, 900–903 (2020).
32. Song, J. C. W., Samutpraphoot, P. & Levitov, L. S. Topological Bloch bands in graphene superlattices. *Proc. Natl Acad. Sci. USA* **112**, 10879–10883 (2015).
33. Po, H. C., Zou, L., Vishwanath, A. & Senthil, T. Origin of Mott insulating behavior and superconductivity in twisted bilayer graphene. *Phys. Rev. X* **8**, 031089 (2018).
34. Zou, L., Po, H. C., Vishwanath, A. & Senthil, T. Band structure of twisted bilayer graphene: Emergent symmetries, commensurate approximants, and Wannier obstructions. *Physical Review B* **98**, 085435 (2018).
35. Liu, J., Liu, J. & Dai, X. Pseudo Landau level representation of twisted bilayer graphene: band topology and implications on the correlated insulating phase. *Phys. Rev. B* **99**, 155415 (2019).
36. Xie, M. & MacDonald, A. H. On the nature of the correlated insulator states in twisted bilayer graphene. *Phys. Rev. Lett.* **124**, 097601 (2020).
37. Kang, J. & Vafek, O. Strong coupling phases of partially filled twisted bilayer graphene narrow bands. *Phys. Rev. Lett.* **122**, 246401 (2019).
38. Liu, S., Khalaf, E., Lee, J. Y. & Vishwanath, A. Nematic topological semimetal and insulator in magic angle bilayer graphene at charge neutrality. Preprint at https://arxiv.org/abs/1905.07409 (2019).
39. Liu, J. & Dai, X. Correlated insulating states and the quantum anomalous Hall phenomena at all integer fillings in twisted bilayer graphene. Preprint at https://arxiv.org/abs/1911.03760 (2020).
40. Wu, F. & Sarma, S. D. Collective excitations of quantum anomalous hall ferromagnets in twisted bilayer graphene. *Phys. Rev. Lett.* **124**, 046403 (2020).
41. Zhang, Y., Jiang, K., Wang, Z. & Zhang, F. Correlated insulating phases of twisted bilayer graphene at commensurate filling fractions: a Hartree-Fock study. Preprint at https://arxiv.org/abs/2001.02476 (2020).
42. Bultinck, N. et al. Ground state and hidden symmetry of magic angle graphene at even integer filling. Preprint at https://arxiv.org/abs/1911.02045 (2019).
43. Dodaro, J. F., Kivelson, S. A., Schattner, Y., Sun, X. Q. & Wang, C. Phases of a phenomenological model of twisted bilayer graphene. *Phys. Rev. B* **98**, 075154 (2018).
44. Xu, C. & Balents, L. Topological superconductivity in twisted multilayer graphene. *Phys. Rev. Lett.* **121**, 087001 (2018).
45. Guinea, F. & Walet, N. R. Electrostatic effects, band distortions, and superconductivity in twisted graphene bilayers. *Proc. Natl Acad. Sci. USA* **115**, 13174–13179 (2018).
46. Liu, C.-C., Zhang, L.-D., Chen, W.-Q. & Yang, F. Chiral Spin Density Wave and d+ i d Superconductivity in the Magic-Angle-Twisted Bilayer Graphene. *Phys. Rev. Lett.* **121**, 217001 (2018).
47. Guo, H., Zhu, X., Feng, S. & Scalettar, R. T. Pairing symmetry of interacting fermions on a twisted bilayer graphene superlattice. *Phys. Rev. B* **97**, 235453 (2018).
48. Lian, B., Wang, Z. & Bernevig, B. A. Twisted bilayer graphene: a phonon-driven superconductor. *Phys. Rev. Lett.* **122**, 257002 (2019).
49. Wu, F., MacDonald, A. H. & Martin, I. Theory of phonon-mediated superconductivity in twisted bilayer graphene. *Phys. Rev. Lett.* **121**, 257001 (2018).
50. Peltonen, T. J., Ojajärvi, R. & Heikkilä, T. T. Mean-field theory for superconductivity in twisted bilayer graphene. *Phys. Rev. B* **98**, 220504 (2018).
51. Mayorov, A. S. et al. Micrometer-scale ballistic transport in encapsulated graphene at room temperature. *Nano Lett.* **11**, 2396–2399 (2011).
52. Stepanov, P. et al. The interplay of insulating and superconducting orders in magic-angle graphene bilayers. Preprint at https://arxiv.org/abs/1911.09198 (2019).
53. Arora, H. S. et al. Superconductivity without insulating states in twisted bilayer graphene stabilized by monolayer WSe_2. Preprint at https://arxiv.org/abs/2002.03003 (2020).
54. Liu, X. et al. Spin-polarized Correlated Insulator and Superconductor in Twisted Double Bilayer Graphene. Preprint at https://arxiv.org/abs/1903.08130 (2019).
55. Codecido, E. et al. Correlated insulating and superconducting states in twisted bilayer graphene below the magic angle. *Sci. Adv.* **5**, eaaw9770 (2019).
56. Moriyama, S. et al. Observation of superconductivity in bilayer graphene/hexagonal boron nitride superlattices. Preprint at https://arxiv.org/abs/1901.09356 (2019).
57. Chen, G. et al. Signatures of tunable superconductivity in a trilayer graphene moiré superlattice. *Nature* **572**, 215–219 (2019).
58. He, M. et al. Tunable correlation-driven symmetry breaking in twisted double bilayer graphene. Preprint at https://arxiv.org/abs/2002.08904 (2020).
59. Choi, Y. et al. Electronic correlations in twisted bilayer graphene near the magic angle. *Nat. Phys* **15**, 1174–1180 (2019).
60. Kerelsky, A. et al. Maximized electron interactions at the magic angle in twisted bilayer graphene. *Nature* **572**, 95–100 (2019).
61. Xie, Y. et al. Spectroscopic signatures of many-body correlations in magic-angle twisted bilayer graphene. *Nature* **572**, 101–105 (2019).
62. Uri, A. et al. Mapping the twist angle and unconventional Landau levels in magic angle graphene. *Nature* **581**, 47–52 (2020).
63. Zondiner, U. et al. Cascade of phase transitions and dirac revivals in magic angle graphene. Preprint at https://arxiv.org/abs/1912.06150 (2019).
64. Wong, D. et al. Cascade of transitions between the correlated electronic states of magic-angle twisted bilayer graphene. Preprint at https://arxiv.org/abs/1912.06145 (2019).
65. McGilly, L. J. et al. Seeing moiré superlattices. Preprint at https://arxiv.org/abs/1912.06629 (2019).
66. Utama, M. I. B. et al. Visualization of the flat electronic band in twisted bilayer graphene near the magic angle twist. Preprint at https://arxiv.org/abs/1912.00587 (2019).
67. Saito, Y., Ge, J., Watanabe, K., Taniguchi, T. & Young, A. F. Decoupling superconductivity and correlated insulators in twisted bilayer graphene. Preprint at https://arxiv.org/abs/1911.13302 (2019).
68. Lee, P. A., Nagaosa, N. & Wen, X.-G. Doping a Mott insulator: Physics of high-temperature superconductivity. *Rev. Mod. Phys.* **78**, 17–85 (2006).
69. Kang, J. & Vafek, O. *Symmetry, maximally localized Wannier States, and a low-energy model for twisted bilayer graphene narrow bands. Phys. Rev. X* **8**, 031088 (2018).
70. Koshino, M. et al. Maximally localized Wannier orbitals and the extended Hubbard Model for twisted bilayer graphene. *Phys. Rev. X* **8**, 031087 (2018).
71. Carr, S., Fang, S., Po, H. C., Vishwanath, A. & Kaxiras, E. Derivation of Wannier orbitals and minimal-basis tight-binding Hamiltonians for twisted bilayer graphene: first-principles approach. *Phys. Rev. Res* **1**, 033072 (2019).
72. Goodwin, Z. A. H., Corsetti, F., Mostofi, A. A. & Lischner, J. Twist-angle sensitivity of electron correlations in moiré graphene bilayers. *Phys. Rev. B* **100**, 121106 (2019).
73. Pizarro, J. M., Rösner, M., Thomale, R., Valentí, R. & Wehling, T. O. Internal screening and dielectric engineering in magic-angle twisted bilayer graphene. *Phys. Rev. B* **100**, 161102 (2019).
74. Liu, X. et al. Tuning electron correlation in magic-angle twisted bilayer graphene using Coulomb screening. Preprint at https://arxiv.org/abs/2003.11072 (2020).
75. Tsuei, C. C. & Kirtley, J. R. Pairing symmetry in cuprate superconductors. *Rev. Mod. Phys.* **72**, 969–1016 (2000).
76. Polshyn, H. et al. Large linear-in-temperature resistivity in twisted bilayer graphene. *Nat. Phys* **15**, 1011–1016 (2019).
77. Cao, Y. et al. Strange metal in magic-angle graphene with near Planckian dissipation. *Phys. Rev. Lett.* **124**, 076801 (2020).
78. Cao, Y. et al. Electric field tunable correlated states and magnetic phase transitions in twisted bilayer-bilayer graphene. *Nature* https://doi.org/10.1038/s41586-020-2260-6 (2020).
79. Burg, G. W. et al. Correlated insulating states in twisted double bilayer graphene. *Phys. Rev. Lett.* **123**, 197702 (2019).
80. Shen, C. et al. Correlated states in twisted double bilayer graphene. *Nat. Phys* https://doi.org/10.1038/s41567-020-0825-9 (2020).
81. Zhang, Z. et al. Flat bands in small angle twisted bilayer WSe2. Preprint at https://arxiv.org/abs/1910.13068 (2019).
82. Zaletel, M. P., Mong, R. S. K., Pollmann, F. & Rezayi, E. H. Infinite density matrix renormalization group for multicomponent quantum Hall systems. *Phys. Rev. B* **91**, 045115 (2015).

83. Carr, S., Fang, S., Jarillo-Herrero, P. & Kaxiras, E. Pressure dependence of the magic twist angle in graphene superlattices. *Phys. Rev. B* **98**, 085144 (2018).
84. Chittari, B. L., Leconte, N., Javvaji, S. & Jung, J. Pressure induced compression of flatbands in twisted bilayer graphene. *Electron. Struct* **1**, 015001 (2018).
85. Chen, G. et al. Tunable correlated Chern insulator and ferromagnetism in a moiré superlattice. *Nature* **579**, 56–61 (2020).

Acknowledgements

We thank K. Hejazi and C. Liu for assistance with preparation of Fig. 1c. L.B. acknowledges support by the NSF CMMT program under award no. DMR-1818533; the US Department of Energy, Office of Science, Basic Energy Sciences under award no. DE-FG02-08ER46524 and the UCSB NSF Quantum Foundry through Q-AMASE-i program award no. DMR-1906325. A.F.Y. acknowledges the support of the US Department of Energy, Office of Science, Basic Energy Sciences under award no. DE-SC0020043 and the UCSB NSF Quantum Foundry through Q-AMASE-i program award no. DMR-1906325. C.R.D. acknowledges the support of the Pro-QM EFRC funded by the US Department of Energy, Office of Science, Basic Energy Sciences under award no. DE-SC0019443. D.K.E. acknowledges support from the Ministry of Economy and Competitiveness of Spain through the 'Severo Ochoa' program for Centres of Excellence in R&D (SE5-0522), Fundació Privada Cellex, Fundació Privada Mir-Puig, the Generalitat de Catalunya through the CERCA program, the H2020 Programme under grant agreement no. 820378, Project: 2D·SIPC and the La Caixa Foundation.

Competing interests

The authors declare no competing interests.

Additional information

Correspondence should be addressed to L.B., D.K.E. or A.F.Y.

Peer review information *Nature Physics* thanks Emanuel Tutuc and Oskar Vafek for their contribution to the peer review of this work.